

Article

Theoretical Investigation on the Selective Hydroxyl Radical-Induced Decolorization of Methylene-Blue-Dyed Polymer Films

Pasika Temeeprasertkij ^{1,*}, Michio Iwaoka ²  and Satoru Iwamori ¹¹ Graduate School of Science and Technology, Tokai University, Kanagawa 259-1292, Japan² Department of Chemistry, Tokai University, Kanagawa 259-1292, Japan

* Correspondence: OCTAD020@cc.u-tokai.ac.jp

Abstract: On the basis of the decolorization caused by the reaction of active oxygen species (AOSs) with methylene blue (MB), our group recently developed colorimetric indicators for hydroxyl radical (OH radical) by embedding MB in polymer thin films made of water-soluble pullulan or sodium alginate. In the present work, to elucidate the reason for the selective decolorization induced by the OH radical compared with other AOSs, such as ozone (O₃) and hydrogen peroxide (H₂O₂), density-functional-theory calculations were performed at the B3LYP/6-31G(d) level for these AOSs and MB and its complexes with pullulan or sodium alginate model molecules. A frontier orbital analysis revealed that the π orbital of MB tends to delocalize on the whole molecule upon complexing with pullulan and sodium alginate, while the energy level is lower than the lowest unoccupied molecular orbital levels of O₃ and H₂O₂ but higher than the singly occupied molecular orbital level of the OH radical. The results support the observation that only the OH radical, as the strongest oxidant, can react with MB in the polymer matrices. The selective decolorization of MB-dyed polymer films by the OH radical is due to not only the steric hindrance in the polymer matrix but also the perturbation of the π orbital of MB through the interaction with the polymer molecules.

Keywords: hydroxyl radical; methylene blue; pullulan; sodium alginate; chemical reactions; density functional theory



Citation: Temeeprasertkij, P.; Iwaoka, M.; Iwamori, S. Theoretical Investigation on the Selective Hydroxyl Radical-Induced Decolorization of Methylene-Blue-Dyed Polymer Films. *Computation* **2022**, *10*, 169. <https://doi.org/10.3390/computation10100169>

Academic Editor: Karlheinz Schwarz

Received: 10 September 2022

Accepted: 16 September 2022

Published: 21 September 2022

Publisher's Note: MDPI stays neutral with regard to jurisdictional claims in published maps and institutional affiliations.



Copyright: © 2022 by the authors. Licensee MDPI, Basel, Switzerland. This article is an open access article distributed under the terms and conditions of the Creative Commons Attribution (CC BY) license (<https://creativecommons.org/licenses/by/4.0/>).

1. Introduction

Active oxygen species (AOSs), such as hydroxyl radical (OH radical), hydrogen peroxide (H₂O₂), and ozone (O₃), are involved in various industrial applications, owing to their extremely strong oxidizing ability [1–4]. Among them, the OH radical has the strongest oxidizing ability and is frequently utilized for the decolorization of dyes. The OH radical is a highly electrophilic species that reacts with the electron-rich sites of organic compounds to cause degradation via complex reactions involving free radicals, which are usually unstable and highly reactive, owing to the presence of an unpaired electron [5,6]. In industry, AOSs have been applied to sterilization processes and surface modifications. For example, the OH radical was recently employed to control wastewater contamination [7–9]. AOSs can be easily generated in the atmosphere via the combination of oxygen and UV light [10,11]. This process has an advantage over other processes because of a low operating cost and a limited production of toxic waste. It is of current interest to apply this easy-to-handle process to degrade organic pollutants.

Previously, we designed several methods toward the development of a sensor that can visually determine the presence or absence of a specific AOS via the decolorization of methylene blue (MB) [3,4], which is a representative organic dye. It is known that the decolorization of MB by AOSs occurs through the decomposition of the benzene ring [11–13]. In pursuit of our project, we recently developed selective indicators for the OH radical by embedding MB in polymer thin films made of pullulan or sodium

alginate (SA) [3,4]. Pullulan and SA thin films are environmentally friendly and edible materials [14–18]. In these matrices, the MB pigment was markedly discolored upon exposure to a high-humidity condition in which a high concentration of OH radical was generated, rendering the thin films transparent. However, the decolorization was hardly observed by exposing the films to O₃ or other AOSs under low-humidity conditions. Thus, the decolorization of the films, i.e., the degradation of MB, occurred only upon reaction with OH radical. To address the index for AOS detection by using the decolorization phenomenon that occurs between AOS and composite membranes, at the atomic interaction level, a quantum chemical calculation was carried out for the molecular complexes formed between MB and a truncated pullulan model (MB/pullulan) at the HF/6-31G(d) level or a sodium alginate model (MB/sodium alginate) at the B3LYP/6-31G(d) level. As a result, experimental observations were reasonably supported by the calculation [1,2]. However, the reason why only the OH radical could decolorize the MB-dyed films remained to be elucidated.

In this paper, the theoretical study was extended to the frontier orbital theory analysis of MB/pullulan and MB/sodium alginate model complexes to gain more insight into the essential factors that control the AOS selectivity observed in the decolorization of MB/pullulan and MB/sodium alginate thin films.

2. Methods

Density functional theory (DFT) [19–21] calculations were performed for the OH radical, O₃, and H₂O₂ as AOSs and MB and its complexes with pullulan or sodium alginate model molecules. The same truncated models as those employed in the previous studies [1,2], i.e., a pentamer of α -D-glucose, which is connected by 1–4 glycosidic bonds, except for the 1–6 glycosidic bond between the second and third glucose units, and a tetramer of two D-mannuronic acid and two L-guluronic acid units linked by 1–4 glycosidic bonds, were used in this study as pullulan and sodium alginate models, respectively. For the MB/pullulan and MB/sodium alginate complexes, ten initial structures were imported from the previous studies [1,2]. The geometries were then fully reoptimized at B3LYP/6-31G(d) in vacuo.

For the MB/pullulan complex (MB/P 1–9), the geometries were further optimized without any constraints at the B3LYP/6-31+G(d,p) level of theory, including diffusion and polarization functions. To evaluate more reliable electronic energies, the dispersion-corrected DFT calculation was performed at the B3PW91/6-31+G(d,p)-GD3 level with Grimme's dispersion correction for each optimized structure. To evaluate the solvent effects, the energy calculations were performed in water by using the SCRF method at the same B3PW91-GD3 level. The complexation energies were evaluated with correction for the basis set superposition error (BSSE) by using the Boys and Simons's method [22,23] at the B3PW91-GD3 level.

For the MB/sodium alginate complex (MB/SA 1–9) the geometries could not be optimized at the B3LYP/6-31+G(d,p) level because of our limited computation resource. Therefore, the geometries fully optimized at the B3LYP/6-31G(d) level were employed for the analyses of the solvent effects and complexation energies.

The Gaussian 16 program suit [24] was employed for the calculation, and the GaussView version 6 [25] was used for the visualization of the molecular structures and molecular orbitals. All the structures were characterized as stationary points, which were confirmed by frequency calculation.

3. Results and Discussion

For the MB/pullulan complex (MB/P), nine structures could be characterized as stationary points at the B3LYP/6-31+G(d,p) level. The obtained structures are given in Supplementary Materials Figure S1. In most of the structures, the pullulan molecule was contorted to form a circular shape, whereas the MB molecule maintains a planar structure owing to the aromatic ring system.

Table 1 summarizes the relative energies and the complexation energies obtained at various calculation levels. At the B3LYP/6-31G(d) level, the relative energies for the nine structures lie in the range from 0 to 31 kcal/mol, while the relative energies lie in the range of 0 to 27, 0 to 29, and 0 to 19 kcal/mol at the B3LYP/6-31+G(d,p), B3PW91/6-31+G(d,p)-GD3, and B3PW91/6-31+G(d,p)-SCRF levels, respectively. The complexation energies with BSSE correction range between -67 kcal/mol (for MB/P 1) and -17 kcal/mol (for MB/P 9).

Table 1. The reactive energies and complexation energies of MB/pullulan (MB/P) complex.

MB/P	Reactive Energy (kcal/mole)				Complexation Energy (kcal/mole)
	B3LYP/6-31G(d)//B3LYP/6-31G(d)	B3LYP/6-31+G(d,p)//B3LYP/6-31G(d)	B3PW91/6-31+G(d,p)//B3LYP/6-31+G(d,p)		
			GD3	in Water (SCRF)	GD3+BSSE
1	0.00	0.00	0.00	0.00	-66.67
2	12.80	11.86	7.32	2.33	-59.18
3	14.39	17.96	9.83	1.66	-39.49
4	13.82	14.17	10.03	2.17	-57.37
5	21.42	22.29	24.29	9.48	-22.22
6	21.16	19.45	25.04	18.79	-41.39
7	30.89	27.08	25.17	14.30	-48.87
8	23.34	23.51	28.59	10.25	-19.11
9	26.62	23.82	29.41	8.38	-17.15

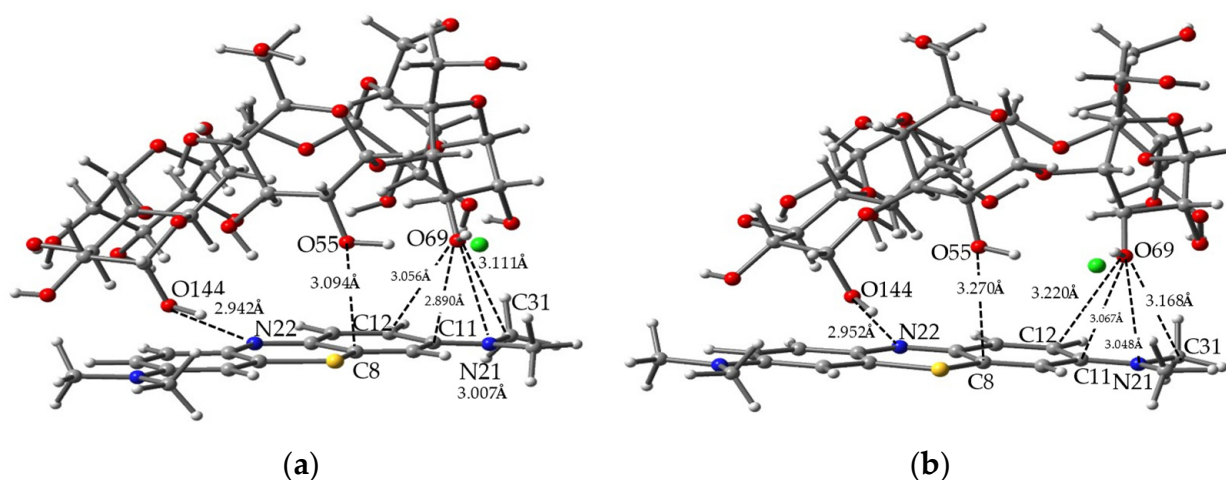
Overall, the relative energies are quite different for each MB/P structure over the various calculation levels. The relative energies obtained in water are especially significantly small compared with those in vacuo. Nevertheless, the order of the stabilities seems to be roughly the same independent of the calculation levels. The order is also consistent with the complexation energies. It should be noted that MB/P 1 is always the most stable structure, with a maximum complexation energy, suggesting that the intermolecular interactions present in MB/P 1 are major forces that stabilize MB in the pullulan matrix.

With regard to the weak intermolecular interactions between MB and pullulan, an OH \cdots N hydrogen bond, a CH \cdots O hydrogen bond, and/or C (π) \cdots O and N (π) \cdots O aromatic interactions were commonly found in all structures. The observed close atomic distances are summarized in Table 2. We set the criterion of the interactions to a slightly larger distance than the sum of the van der Waals radii (i.e., Σ (vdW) + 0.2 Å) [26]. Table 2 shows the slight changes in the atomic distances depending on the calculation level, i.e., the basis sets employed. However, the differences were small, suggesting that overall complex structures did not change significantly by including diffusion and polarization functions. This can be visually seen for the molecular structures of MB/P 4 shown in Figure 1.

In the complex of MB/P 4, there are three kinds of intermolecular interactions. The first one is an OH \cdots N hydrogen bond between O144 of pullulan and N22 of MB. The second one is an aromatic interaction between O55 of pullulan and C8 of MB. The third one is a mixture of an aromatic interaction observed between O69 of pullulan and C11, C12, and N21 of MB and a CH \cdots O hydrogen bond observed between C31 and O69, as seen in Figure 1. Although the atomic distances become slightly larger at the B3LYP/6-31+G(d,p) level, these interactions are kept remaining. Similarly, the molecular structures of MB/P 1-9 obtained at the B3LYP/6-31+G(d,p) level were similar to those obtained at the B3LYP/6-31G(d) level (see Supplementary Figure S1).

Table 2. Intermolecular interactions observed for MB/pullulan (MB/P) complex.

MB/P	N...O				C...O			
	Position	Distance (Å)		Difference	Position	Distance (Å)		Difference
		B3LYP/ 6-31G(d)	B3LYP/ 6-31+G(d,p)			B3LYP/ 6-31G(d)	B3LYP/ 6-31+G(d,p)	
1	none	–	–	–	C2,O55	3.141	3.503	+0.36
2	none	–	–	–	C35,O138	3.191	5.165	+1.97
					C3,O144	3.253	3.311	+0.06
3	none	–	–	–	C23,O69	3.313	3.333	+0.11
					C13,O55	3.183	3.350	+0.17
					C2,O120	3.191	3.349	+0.16
					C1,O120	3.224	3.758	+0.53
4	N22,O144	2.942	2.952	+0.01	C11,O69	3.229	3.393	+0.16
					N21,O69	3.007	3.048	+0.04
					C11,O69	2.890	3.067	+0.18
					C12,O69	3.056	3.220	+0.16
					C8,O55	3.094	3.270	+0.18
5	N22,O69	2.990	2.974	−0.02	C31,O69	3.111	3.168	+0.06
					N22,O55	3.050	3.081	+0.03
6	none	–	–	–	C5,O69	3.159	3.226	+0.07
					C31,O138	3.191	3.522	+0.33
7	N20,O132	3.205	3.341	−0.14	C27,O123	3.255	3.722	+0.47
					C23,O123	3.284	3.372	+0.09
8	N22,O144	2.817	2.838	+0.02	none	–	–	–
9	N22,O53	2.954	2.844	−0.11	none	–	–	–

**Figure 1.** Molecular structures of MB/P 4: (a) optimized at the B3LYP/6-31G(d) level and (b) optimized at the B3LYP/6-31+G(d,p) level. Weak intermolecular interactions observed are shown with broken lines, with the distances in Å. (Blue ball = nitrogen (N), gray ball = carbon (C), yellow ball = sulfur (S), green ball = chlorine (Cl), red ball = oxygen (O), and white ball = hydrogen (H)).

For the MB/sodium alginate complex (MB/SA), the structures could not be optimized at the B3LYP/6-31+G(d,p) level. However, as seen in the case of the MB/P complex, the use of a smaller basis set, i.e., 6-31G(d), would give reasonable geometries for the intermolecular interactions. We, therefore, employed the molecular structures obtained at the B3LYP/6-31G(d) level for the analysis of the MB/SA complex structures. The obtained nine structures are shown in Supplementary Figure S2.

Table 3 summarizes the relative energies and complexation energies. At the B3LYP/6-31G(d) level, the relative energies were in a range of 0 to 24 kcal/mole. In order to obtain more reliable energies for MB/SA 1–9, a single-point energy calculation was performed at higher levels of theory, using the structures obtained at the B3LYP/6-31G(d) level. The

relative energies thus obtained lie in the range from 0 to 18 kcal/mole, 0 to 32 kcal/mole, and 0 to 17 kcal/mole at the B3LYP/6-31+G(d,p), B3PW91/6-31+G(d,p)-GD3, and B3PW91/6-31+G(d,p)-SCRF levels, respectively. Like the case of the MB/P complex, the magnitude of the relative energies was quite different depending on the calculation level. However, the order did not change significantly for MB/SA. The order of the complexation energies was also consistent with that of the relative energies. The complexation energies ranged from -93 to -52 kcal/mol, which is larger than that observed for MB/P 1, suggesting that MB is more stabilized in the sodium alginate matrix than in the pullulan matrix.

Table 3. The reactive energies and complexation energies of MB/sodium alginate (MB/SA) complex.

MB/SA	Reactive Energy (kcal/mole)				Complexation Energy (kcal/mole)
	B3LYP/6-31G(d)//B3LYP/6-31G(d)	B3LYP/6-31+G(d,p)//B3LYP/6-31G(d)	B3PW91/6-31+G(d,p)//B3LYP/6-31G(d)		
			GD3	in Water (SCRF)	
1	0.00	0.00	0.00	0.00	-93.19
2	5.53	4.35	9.25	4.17	-69.54
3	6.75	5.66	8.68	1.55	-68.69
4	8.56	1.19	16.71	0.67	-78.52
5	12.16	8.18	13.00	2.75	-87.91
6	15.90	9.59	28.00	14.48	-57.42
7	17.12	10.05	31.90	17.45	-52.18
8	21.29	13.97	27.32	8.86	-53.13
9	24.24	17.80	29.93	9.52	-60.17

Figure 2 shows the molecular structures of MB/SA 1 and 2. Several kinds of interaction can be seen in these structures. In MB/SA 1, $S(\pi)\cdots O$ and $C(\pi)\cdots O$ aromatic interactions are present between O106 of SA and S19 and C3 of MB. A $CH\cdots O$ hydrogen bond is present between O121 of SA and C27 of MB. In MB/SA 2, an $OH\cdots N$ hydrogen bond is present between N20 of MB and O117 of SA, which also has close contact with C1. Near this hydrogen bond, there is a $C(\pi)\cdots O$ aromatic interaction between C2 of MB and O113 of SA. On the other side of the complex, there is a weak $C\cdots O$ interaction between C35 of MB and O59 of SA. The SA molecule is slightly contorted, which is in contrast to the molecular structure of SA in MB/SA 1.

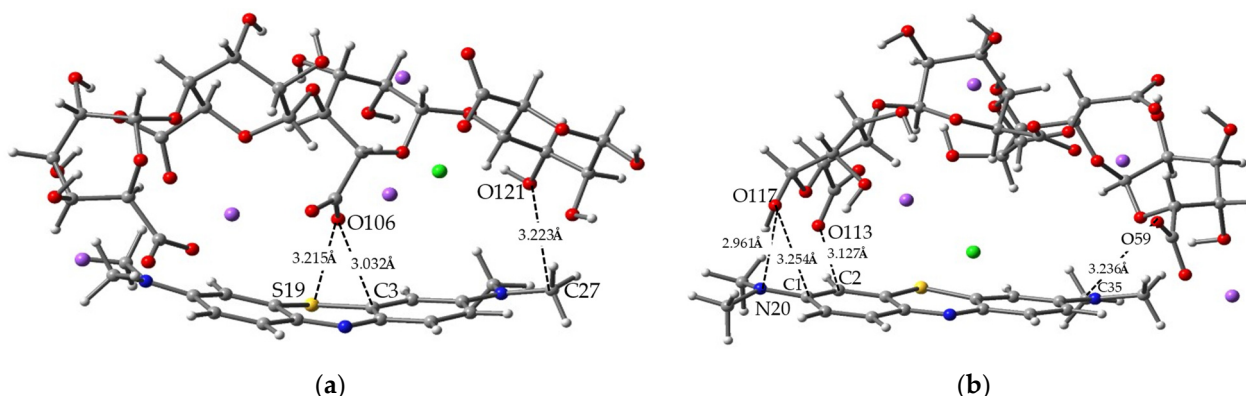


Figure 2. (a) The molecular structure of MB/SA 1 obtained at the B3LYP/6-31g(d) level. (b) The molecular structure of MB/SA 2 obtained at the B3LYP/6-31g(d) level. Weak intermolecular interactions observed are shown with broken lines with the distances in Å. (Blue ball = nitrogen (N), gray ball = carbon (C), yellow ball = sulfur (S), green ball = chlorine (Cl), red ball = oxygen (O), white ball = hydrogen (H), and purple ball = sodium (Na).

The interaction modes identified between MB and SA for MB/SA 1–9 are summarized in Table 4. The same criterion that was used for the MB/P complex, i.e., $\Sigma(\text{vdW}) + 0.2 \text{ \AA}$, was employed for the analysis. A careful investigation into the molecular structures of the complex (see Supplementary Figure S2) led us to identify the representative interaction modes, i.e., CH \cdots O hydrogen bond and S(π) \cdots O and C(π) \cdots O aromatic interactions. For example, a CH \cdots O hydrogen bond was found in MB/SA 1–5, 7, and 9, while a S(π) \cdots O and C(π) \cdots O aromatic interactions were found in MB/SA 1, 5, and 8. As in other interaction modes, there were two S \cdots O chalcogen bonds in MB/SA 4. For MB/SA 6, there was no such obvious interaction, suggesting that van der Waals, or dispersion, interaction should also contribute to the stability of the MB/SA complex.

Table 4. Intermolecular interactions observed for MB/sodium alginate (MB/SA) complex.

MB/SA	N \cdots O		C \cdots O		S \cdots O	
	B3LYP/6-31G(d)					
	Position	Distance (Å)	Position	Distance (Å)	Position	Distance (Å)
1	none	none	C3,O106 C27,O121	3.032 3.223	S19,O106	3.215
2	N20,O117	2.961	C2,O113 C35,O59 C1,O117	3.127 3.236 3.254	none	none
3	none	none	C2,O113 C35,O59	3.200 3.201	none	none
4	none	none	C2,O63	3.243	S19,O59 S19,O63	3.256 3.118
5	none	none	C8,O108 C31,O62 C12,O62	3.034 3.244 3.299	S19,O108	3.477
6	none	none	None	none	none	none
7	N20,O57	3.176	C27,O57	3.193	none	none
8	none	none	C8,O60 C7,O60	2.956 3.165	S19,O60	3.269
9	none	none	C35,O60	3.194	none	none

Subsequently, the frontier orbitals were analyzed to identify the factors that control the reactions of AOSs with MB. Table 5 summarizes the results obtained for a series of parameters associated with the decolorization of MB, i.e., the lowest unoccupied molecular orbital (LUMO) and highest occupied molecular orbital (HOMO) energies (E_{LUMO} and E_{HOMO} , respectively), the energy gap (E_g), hardness (η) [27,28], softness (σ), and electronegativity (χ) of OH radical, H₂O₂, and O₃. In the case of the OH radical, the singly occupied molecular orbital (SOMO) accepts an electron from the substrate. Therefore, the SOMO is utilized as the LUMO for convenience. It is worth noting that the OH radical is the most electrophilic and softest among the AOSs evaluated.

Table 6 summarizes the reaction parameters obtained for MB, pullulan, and sodium alginate models and MB/pullulan and MB/sodium alginate complexes. The parameters for the complexes are those obtained for MB/pullulan 1 in Supplementary Figure S1a and MB/sodium alginate 1 in Figure 2a. The smaller E_g of MB ($E_g = 2.49 \text{ eV}$) compared with that of pullulan ($E_g = 7.54 \text{ eV}$) and sodium alginate ($E_g = 3.35 \text{ eV}$) suggests that MB is more reactive than the matrix polymers. When MB forms a complex with pullulan or sodium alginate, the E_g decreases slightly ($E_g = 2.49$ and 2.41 eV , respectively), suggesting that MB maintains its reactivity, or even is slightly activated, in the matrices. In consonance with this result, the hardness of MB decreases in the complexes. Thus, the frontier orbital energy analysis supports the argument that pullulan and sodium alginate can be utilized as protective layers for the degradation of MB.

Table 5. Reaction parameters for the active oxygen species (AOSs) obtained via the frontier orbital analysis at the B3LYP/6-31G(d) level of theory.

Property	Formula	AOS		
		OH Radical	H ₂ O ₂	O ₃
LUMO energy (eV)	E_{LUMO}^a	−6.59 ^a	0.57	−4.90
HOMO energy (eV)	E_{HOMO}	−7.26	−6.71	−8.98
Energy gap (eV)	$E_g = E_{\text{LUMO}} - E_{\text{HOMO}}$	0.67	7.27	4.08
Hardness	$\eta = E_g/2$	0.34	3.64	2.04
Softness	$\sigma = 1/\eta$	2.98	0.27	0.49
Electronegativity	$\chi = -(E_{\text{LUMO}} + E_{\text{HOMO}})/2$	6.93	3.07	6.94

^a The SOMO energy level was used as the LUMO energy level.

Table 6. Reaction parameters for methylene blue (MB) and its complexes with pullulan or sodium alginate obtained via the frontier orbital analysis at the B3LYP/6-31g(d) level of theory.

Property	Structure				
	MB	Pullulan	Sodium Alginate	MB/Pullulan	MB/Sodium Alginate
LUMO energy (eV)	−3.23	0.81	−2.05	−3.49	−3.21
HOMO energy (eV)	−5.72 ^a	−6.73	−5.40	−5.97	−5.63
Energy gap (eV)	2.49	7.54	3.35	2.49	2.41
Hardness	1.25	3.77	1.68	1.24	1.21
Softness	0.80	0.27	0.60	0.80	0.83
Electronegativity	4.48	2.96	3.73	4.73	4.42

^a The HOMO-3 energy level is shown because the HOMO, HOMO-1, and HOMO-2 are localized at the chloride anion.

Interestingly, the HOMO levels of MB/pullulan (−5.97 eV) and MB/sodium alginate (−5.63 eV) are higher than the SOMO level of the OH radical (−6.59 eV), suggesting that the MB-dyed polymers are easily oxidized by the action of the OH radical. Moreover, the slightly higher HOMO level of MB/sodium alginate compared with that of MB/pullulan suggests that MB is more reactive in the sodium alginate matrix than in the pullulan matrix. Meanwhile, the LUMOs of H₂O₂ (0.57 eV) and O₃ (−4.90 eV) are higher in energy than the HOMOs of MB/pullulan and MB/sodium alginate, indicating that these AOSs cannot oxidize the MB-dyed polymers. Thus, the selective decolorization of the MB-dyed thin films by the OH radical can be reasonably explained by the frontier orbital theory.

Figure 3 shows the HOMO-3 of MB, along with the HOMOs of the MB/pullulan 1 and MB/sodium alginate 1 complexes. These orbitals consist of a π orbital of MB, which is involved in the reaction with an oxidant during the decolorization. In MB, the orbital tends to localize in the phenothiazinium structure, whereas it is delocalized on the whole MB molecule in the complexes. These changes in the orbital shape, which probably facilitate the reaction of the OH radical with MB in the matrix, stem most likely from the weak atomic interactions between MB and pullulan or sodium alginate. The results suggest that the delocalization of the HOMO of MB would also explain the observed easier reaction of OH radical in the polymer matrix.

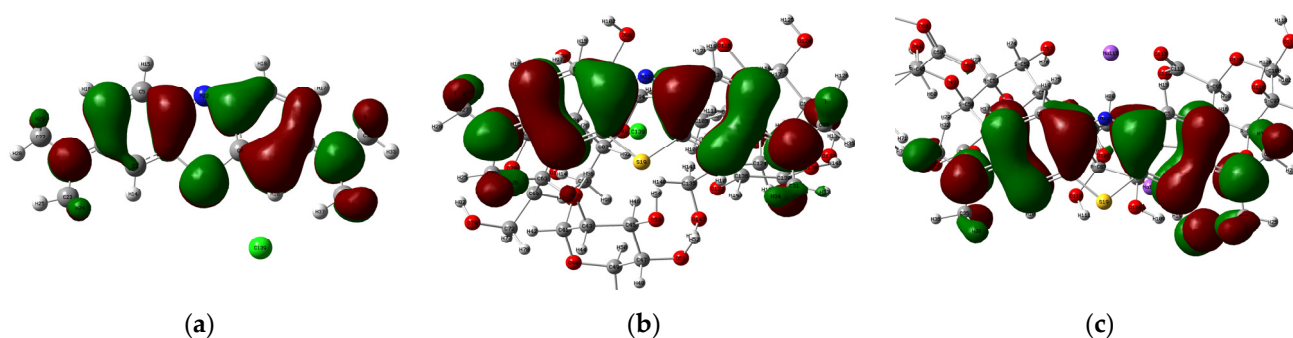


Figure 3. Shapes of molecular orbitals obtained at the B3LYP/6-31G(d) level of theory: (a) HOMO-3 of methylene blue (MB), (b) HOMO of MB/P 1, and (c) HOMO of MB/SA 1.

4. Conclusions

In this study, DFT calculations were performed on MB/pullulan and MB/sodium alginate model complexes at the B3LYP/6-31g(d), B3LYP/6-31+g(d,p), and B3PW91/6-31+g(d,p) levels of theory. The result indicates that the relative energies obtained in water are significantly small compared with those in vacuo. The stabilities seem to be roughly the same independent of the calculation levels. The order is also consistent with the complexation energies. MB/P 1 and MB/SA 1 are always the most stable structure with maximum complexation energy. The frontier-orbital-energy analysis revealed that the π orbital level of MB is located at a lower energy level than the LUMO levels of O_3 and H_2O_2 but at a higher energy level than the SOMO level of the OH radical and that this situation is maintained in the pullulan and sodium alginate matrices. It was also found that the π orbital of MB is more delocalized in the matrices, owing to the interaction with the polymer molecules. These results reasonably support the experimental observation that only the OH radical, which exhibits the strongest oxidizing ability among the AOSs evaluated, can decolorize the MB-dyed polymer thin films [1]. Thus, it can be concluded that the selective decolorization induced by the OH radical is due to not only the steric hindrance for larger AOSs in the polymer matrix but also the perturbation of the π orbital of MB via the interaction with the polymer molecules in the matrix. This study provides useful insights for the development of new AOS indicators or sensors that react selectively with a specific AOS.

Supplementary Materials: The following supporting information can be downloaded at <https://www.mdpi.com/article/10.3390/computation10100169/s1>. Figure S1: Molecular structures of MB/P 1-9. Figure S2: MB/SA 1-9. These materials are available free of charge from the publisher's website.

Author Contributions: Conceptualization, P.T. and S.I.; methodology, P.T., M.I. and S.I.; software, P.T., M.I. and S.I.; validation, P.T. and S.I.; formal analysis, P.T.; investigation, P.T.; resources, P.T.; data curation, P.T.; writing—original draft preparation, P.T. and S.I.; writing—review and editing, P.T., M.I. and S.I.; visualization, P.T. and S.I.; supervision, P.T. and S.I.; project administration, P.T. and S.I.; funding acquisition, S.I. All authors have read and agreed to the published version of the manuscript.

Funding: This research received no external funding.

Institutional Review Board Statement: Not applicable.

Informed Consent Statement: Not applicable.

Data Availability Statement: Not applicable.

Conflicts of Interest: The authors declare that there is no conflict of interest.

Sample Availability: Samples of the compound's OH radical, H_2O_2 , ozone, methylene blue, sodium alginate, and pullulan are available from the authors.

References

1. Temeepresertkij, P.; Yenchit, S.; Iwaoka, M.; Iwamori, S. Interactions between Methylene Blue and Pullulan According to Molecular Orbital Calculations. *IEEJ Trans. Fundam. Mater.* **2020**, *140*, 529–533. [[CrossRef](#)]
2. Temeepresertkij, P.; Iwaoka, M.; Iwamori, S. Molecular Interactions between Methylene Blue and Sodium Alginate Studied by Molecular Orbital Calculations. *Molecules* **2021**, *26*, 7029. [[CrossRef](#)] [[PubMed](#)]
3. Yenchit, S.; Yamanaka, H.; Temeepresertkij, P.; Oda, Y.; Kanie, O.; Okamura, Y.; Inazu, T.; Iwamori, S. Chemical Stability of a Colorimetric Indicator Based on Sodium Alginate Thin Film and Methylene Blue Dye upon Active Oxygen Species Exposure. *Jpn. J. Appl. Phys.* **2020**, *59*, SDDF09. [[CrossRef](#)]
4. Yenchit, S.; Tadokoro, Y.; Iwamori, S. Measuring Active Oxygen Species across a Nonwoven Fabric Using a Pullulan-Mixed Methylene Blue Thin Film and Electron Spin Resonance. *IEEJ Trans. Sens. Micromach.* **2019**, *139*, 54–60. [[CrossRef](#)]
5. Kumar, A.; Pottiboyina, V.; Sevilla, M.D. Hydroxyl Radical (OH•) Reaction with Guanine in an Aqueous Environment: A DFT Study. *J. Phys. Chem. B* **2011**, *115*, 15129–15137. [[CrossRef](#)]
6. Çakmak, E.; Isin, D.O. A Theoretical Evaluation on Free Radical Scavenging Activity of 3-Styrylchromone Derivatives: The DFT Study. *J. Mol. Model.* **2020**, *26*, 98. [[CrossRef](#)]
7. Hassaan, M.A.; Nemr, A.E.; Madkour, F.F. Testing the advanced oxidation processes on the degradation of Direct Blue 86 dye in wastewater. *Egypt. J. Aquat. Res.* **2017**, *43*, 11–19. [[CrossRef](#)]
8. Miklos, D.B.; Remy, C.; Jekel, M.; Linden, K.G.; Drewes, J.E.; Hübner, U. Evaluation of advanced oxidation processes for water and wastewater treatment. *Water Res.* **2018**, *139*, 118–131. [[CrossRef](#)]
9. Kuang, Y.; Zhang, X.; Zhou, S. Adsorption of Methylene Blue in Water onto Activated Carbon by Surfactant Modification. *Water* **2020**, *12*, 587. [[CrossRef](#)]
10. Yoshino, K.; Matsumoto, H.; Iwasaki, T.; Kinoshita, S.; Noda, K.; Oya, K.; Iwamori, S. Investigation of a Sterilization System Using Active Oxygen Species Generated by Ultraviolet Irradiation. *Biocontrol Sci.* **2015**, *20*, 11–18. [[CrossRef](#)]
11. Oya, K.; Watanabe, R.; Soga, Y.; Ikeda, Y.; Nakamura, T.; Iwamori, S. Effect of humidity conditions on active oxygen species generated under ultraviolet light irradiation and etching characteristics of fluorocarbon polymer. *J. Photochem. Photobiol. A Chem.* **2015**, *298*, 33–39. [[CrossRef](#)]
12. Murakami, Y.; Oguchi, T.; Hashimoto, K.; Nakamura, A.; Sakai, Y.; Ando, H. Density functional study of the phenylethyl + O₂ reaction: Kinetic analysis for the low-temperature autoignition of ethylbenzenes. *Int. J. Quantum Chem.* **2012**, *112*, 1968–1983. [[CrossRef](#)]
13. Tokmakov, I.V.; Kim, G.-S.; Kislov, V.V.; Mebel, A.M.; Lin, M.C. The reaction of phenyl radical with molecular oxygen: A G2M study of the potential energy surface. *J. Phys. Chem. A* **2005**, *109*, 6114–6127. [[CrossRef](#)]
14. Yan, J.; Li, Z.; Zhang, J.; Qiao, C. Preparation and Properties of Pullulan Composite Films. *Adv. Mater. Res.* **2012**, *476–478*, 2100–2104. [[CrossRef](#)]
15. Li, Y.; Yokoyama, W.; Wu, J.; Ma, J.; Zhong, F. Properties of Edible Films based on Pullulan–Chitosan Blended Film-Forming Solutions at Different pH. *R. Soc. Chem.* **2015**, *5*, 105844–105850. [[CrossRef](#)]
16. Wang, Z.; Yang, H.; Zhu, Z. Study on the Blends of Silk Fibroin and Sodium Alginate: Hydrogen Bond Formation, Structure and Properties. *Polymer* **2019**, *163*, 144–153. [[CrossRef](#)]
17. Lan, W.; He, L.; Liu, Y. Preparation and Properties of Sodium Carboxymethyl Cellulose/Sodium Alginate/Chitosan Composite Film. *Coatings* **2018**, *8*, 291. [[CrossRef](#)]
18. Harnsilawat, T.; Pongsawatmanit, R.; McClements, D.J. Characterization of β -Lactoglobulin–Sodium Alginate Interactions in Aqueous Solutions: A Calorimetry, Light Scattering, Electrophoretic Mobility and Solubility Study. *Food Hydrocoll.* **2006**, *20*, 577–585. [[CrossRef](#)]
19. Pascoe, D.J.; Ling, K.B.; Cockroft, S.L. The Origin of Chalcogen-Bonding Interactions. *Am. Chem. Soc.* **2017**, *139*, 15160–15167. [[CrossRef](#)]
20. Balachandar, S.; Dhandapani, M.; Enoch, I.V.M.V.; Suganthi, S. Structural Analysis, Molecular Docking and DFT Calculations of Bis (Pyrazolium Picrate) Monohydrate Interaction with Calf Thymus DNA and Microbes. *ChemistrySelect* **2017**, *2*, 9298–9311. [[CrossRef](#)]
21. Okutsu, N.; Shimamura, K.; Shimizu, E.; Shulga, S.; Danilov, V.I.; Kurita, N. DFT Study on the Attacking Mechanisms of H and OH Radicals to G-C and A-T Base Pairs in Water. In Proceedings of the AIP Conference Proceedings 1709, Aichi, Japan, 22–23 October 2015; AIP Publishing LLC: Huntington, NY, USA, 2016; pp. 020006-1–020006-14.
22. Boys, S.F.; Bernardi, F. The calculation of small molecular interactions by the differences of separate total energies. Some procedures with reduced errors. *Mol. Phys.* **1970**, *19*, 553–566. [[CrossRef](#)]
23. Simon, S.; Duran, M.; Dannenberg, J.J. How does basis set superposition error change the potential surfaces for hydrogenbonded dimers? *J. Chem. Phys.* **1996**, *105*, 11024. [[CrossRef](#)]
24. Frisch, M.J.; Trucks, G.W.; Schlegel, H.B.; Scuseria, G.E.; Robb, M.A.; Cheeseman, J.R.; Scalmani, G.; Barone, V.; Petersson, G.A.; Nakatsuji, H. *Gaussian 16*; Revision C.01; Gaussian, Inc.: Wallingford, CT, USA, 2016.
25. Dennington, R.; Keith, A.T.; Millam, M.J. *GaussView*; Version 6.1; Semichem Inc.: Shawnee, KS, USA, 2016.
26. Batsanov, S.S. Calculation of van der Waals radii of atoms from bond distances. *J. Mol. Struct. THEOCHEM* **1999**, *468*, 151–159. [[CrossRef](#)]

-
27. Parr, R.G.; Pearson, R.G. Absolute Hardness: Companion Parameter to Absolute Electronegativity. *Am. Chem. Soc.* **1983**, *105*, 7512–7516. [[CrossRef](#)]
 28. Pearson, R.G. Absolute Electronegativity and Hardness: Application to Inorganic Chemistry. *Inorg. Chem.* **1988**, *27*, 734–740. [[CrossRef](#)]